



Computer Programs in Physics

## COLOSS: Complex-scaled Optical and couLOmb Scattering Solver

Junzhe Liu, Jin Lei <sup>ID</sup>\*, Zhongzhou Ren

School of Physics Science and Engineering, Tongji University, Shanghai 200092, China



## ARTICLE INFO

The review of this paper was arranged by Prof. David W. Walker

## Keywords:

Complex scaling  
Scattering theory  
Nuclear reaction  
Optical potential

## ABSTRACT

We introduce COLOSS, a program designed to address the scattering problem using a bound-state technique known as complex scaling. In this method, the oscillatory boundary conditions of the wave function are transformed into exponentially decaying ones, accommodating the long-range Coulomb interaction. The program implements the general local optical potential and the Perey-Buck non-local optical potential, with all potential parameters included in a well-designed input format for ease of use. The design offers users direct access to compute  $S$ -matrices and cross-sections for scattering processes involving a projectile of any spin interacting with a spin-0 target. We provide thorough discussions on the precision of Lagrange functions and their benefits in evaluating matrix elements. Additionally, COLOSS incorporates two distinct rotation methods, making it adaptable to potentials without analytical expressions. Comparative results demonstrate that COLOSS achieves high accuracy when compared with the direct integration method, Numerov, underscoring its utility and effectiveness in scattering calculations.

## Program summary

*Program Title:* COLOSS

*CPC Library link to program files:* <https://doi.org/10.17632/ph4m98rvp2.1>

*Developer's repository link:* <https://github.com/jinleiphys/COLOSS>

*Licensing provisions:* GPLv3

*Programming language:* Fortran

*Nature of problem:* The study of elastic scattering between nuclei is a fundamental problem in nuclear physics, key to understanding nuclear interactions and structure. Traditional methods for solving the Schrödinger equation in such contexts often require imposing boundary conditions at large distances, which can be computationally challenging and prone to inaccuracies, especially for reactions involving strong Coulomb interactions and complex potentials. The complex scaling method offers a robust alternative by transforming the scattered wave function from an oscillatory to an exponentially decaying form, thus eliminating the need for boundary conditions. However, implementing this method requires careful numerical handling and validation of the analytic properties of the involved potentials, such as the Woods-Saxon function, on the complex plane. Additionally, ensuring numerical stability and accuracy across different rotational techniques and integration methods is crucial. This study addresses these challenges by developing a program that leverages the complex scaling method, providing a flexible and accurate tool for calculating elastic scattering between nuclei. The program's ability to handle various optical model potentials and its validation against established methods like Numerov underscores its utility and reliability in nuclear physics research.

*Solution method:* To address the challenges in calculating elastic scattering between nuclei, we utilize the complex scaling method, which transforms the Schrödinger equation to simplify boundary conditions by converting the radial coordinate into the complex plane. This transformation changes the wave function from oscillatory to exponentially decaying. Our approach includes validating results against traditional methods like the Numerov algorithm to ensure accuracy. Additionally, we develop a flexible computational program capable of handling various optical model potentials, such as the Woods-Saxon potential, and performing complex scaling and integration efficiently. This method provides a robust, accurate, and computationally efficient solution for studying elastic scattering in nuclear physics.

*Additional comments including restrictions and unusual features:* Our method, while effective, has some restrictions and unusual features. The complex scaling method requires careful handling to avoid numerical instabilities,

\* Corresponding author.

E-mail address: [jinl@tongji.edu.cn](mailto:jinl@tongji.edu.cn) (J. Lei).

<https://doi.org/10.1016/j.cpc.2025.109568>

Received 1 July 2024; Received in revised form 2 February 2025; Accepted 28 February 2025

especially at large radial distances. Gauss-Legendre quadrature, chosen for its convergence, demands precise selection of points and weights. The computational program's flexibility to handle various optical model potentials, like the Woods-Saxon potential, adds complexity and requires thorough validation. Additionally, large-scale simulations may require significant computational resources. Despite these challenges, our approach provides precise and efficient solutions for elastic scattering in nuclear physics, though users must be cautious of potential numerical instabilities and complexities.

## 1. Introduction

Nuclear reactions play a crucial role in advancing our understanding of the synthesis of nuclei and the properties of dense matter, particularly as observed in neutron stars [1]. These reactions are fundamental to various astrophysical processes, including those occurring in stellar environments and during explosive events like supernovae. By investigating rare isotopes, researchers can gain insights into the mechanisms of nucleosynthesis [2]—the formation of new atomic nuclei from pre-existing nucleons (protons and neutrons)—and the behavior of matter under extreme conditions, such as those found in neutron stars. Understanding these reactions not only illuminates the origins of elements in the universe but also enhances our knowledge of fundamental nuclear physics and the behavior of matter at high densities.

A robust theoretical framework is essential for the accurate interpretation of nuclear reaction processes. Unlike the bound state problem, where the system's wave function exhibits an exponential decay boundary condition and thus remains localized in space, scattering problems present a primary challenge due to the non-localized nature of the wave function. This challenge is particularly pronounced when considering systems with more than two particles, where the boundary conditions become extremely complicated. In such cases, the wave function does not simply decay to zero but extends infinitely, making the problem much more difficult to handle.

Solving the scattering problem in configuration space with these complex boundary conditions requires sophisticated mathematical and numerical techniques. The non-localized nature of the wave functions in scattering problems means that they do not vanish at large distances but instead oscillate, reflecting the continuous spectrum of the system. This introduces significant difficulties in defining and implementing appropriate boundary conditions for the wave functions.

In light of these challenges, a compelling question emerges: how can bound-state-like techniques be applied to tackle scattering problems? This concept dates back to Wigner's R-matrix theory [3,4], which connects bound-state and scattering problems by dividing the configuration space into an internal region with strong interactions and an external region where particles are asymptotically free. In the internal region, wave functions are treated using bound-state methods to solve the Schrödinger equation. The R-matrix, defined at the boundary, encapsulates the internal interactions and matches the internal solutions to the asymptotic solutions in the external region. This simplifies the scattering problem using bound-state-like techniques.

In addition, several other bound-state-like techniques have been developed to address the complexities of scattering problems. Notable among these are the Lorentz Integral Transform (LIT) [5], the complex energy (CE) [6,7], and the complex scaling (CS) [8,9]. For a more comprehensive overview of these methods, readers are referred to Ref. [10]. Among these techniques, the CS method is often considered the most powerful tool for directly connecting scattering with bound state problems. The CS method involves a transformation of the coordinate space into the complex plane, which effectively converts the scattering states into bound-like states. This transformation simplifies the treatment of the asymptotic boundary conditions, allowing for the use of bound-state techniques to solve scattering problems.

The CS method, initially introduced by D.R. Hartree et al. [11] for studying radio wave propagation in the atmosphere, saw a resurgence in the 1960s when Nuttall and Cohen proposed a similar approach to

address scattering problems above the breakup threshold [12]. However, due to historical reasons, these pioneering works were interrupted. Building upon their groundwork, the complex scaling method was revisited and applied to solve resonance problems in atomic and molecular physics [13,14], subsequently proving to be a valuable tool in quantum physics for determining the half-life of resonance states [15,16].

The method's utility quickly expanded to nuclear physics, particularly given that many exotic nuclei are unstable and exist in resonance states. The CS method is widely used to find the resonance state of cluster nuclei and determine their half-lives. While proficient at identifying bound and resonance states, the complex scaling method encounters challenges with long-range interactions, notably in scattering scenarios involving the Coulomb force [17,18], which are crucial for describing collisions with heavy nuclei. Recent advancements have adapted the method to address these long-range forces [8,19,20].

In this study, we present a computer code written in the Fortran language to provide a solver for the two-body scattering problem with comprehensive treatment of long-range Coulomb potentials and complex optical potentials. The general local optical model potential and the Perey-Buck non-local optical potential are implemented. To make the program applicable to a wider range of potential inputs, we consider both cases where the potential has a clear analytical form and where the potential is given in a numerical form, such as those obtained from Fourier transforms in momentum space or from folding models. We have introduced two different rotation methods: rotating the basis function or rotating the Hamiltonian. The first method can be used for all cases of the potential, whereas the latter is simpler and can only be applied to potentials with analytical forms. We have developed a user-friendly input format using Fortran namelist to simplify code utilization and included five diverse examples under varying conditions to facilitate easy initiation.

The paper is organized as follows: In Sec. 2, we provide a comprehensive overview of the theoretical framework concerning the application of the complex scaling method to quantum scattering theory and the numerical techniques involved in its implementation. Sec. 3 presents a detailed description of the program, encompassing its structure, workflow, as well as input and output files. Additionally, five different examples concerning various conditions of the program are shown in Sec. 4 to help users quickly start using the code. Finally, we conclude with remarks on the complex scaling method in Sec. 5.

## 2. Theoretical framework

### 2.1. Complex scaling method

The Complex Scaling (CS) method is a powerful technique used to handle continuum states in quantum mechanics. These states are characterized by wave functions that are not square integrable, meaning they do not vanish at infinity and thus cannot be normalized in the usual sense. To address this, the CS method employs a transformation that renders these exponentially divergent wave functions square integrable, making them more manageable for analysis and computation.

The key idea behind complex scaling is to rotate the coordinate along which the divergence occurs into the complex plane. This rotation reduces the oscillations in the wave functions, making them easier to handle. As a result, the wave functions become square integrable. This approach is also known as the complex coordinate method [21].

Mathematically, the complex scaling operation is represented by the transformation:

$$r \rightarrow r e^{i\theta}, \quad (1)$$

where  $r$  is the radial coordinate and  $\theta$  is a scaling angle. This transformation rotates the coordinate  $r$  by an angle  $\theta$  in the complex plane.

The corresponding operator for this rotation transformation can be expressed as:

$$\hat{S}(\theta) = e^{i\theta/2} e^{i\theta x \frac{\partial}{\partial x}}, \quad (2)$$

where  $\hat{S}(\theta)$  is the scaling operator. When we apply this operator to a wave function  $\Psi(r)$ , we obtain:

$$\hat{S}(\theta)\Psi(r) = e^{i\theta/2}\Psi(re^{i\theta}). \quad (3)$$

This transformation modifies the wave function in such a way that it becomes square integrable, facilitating the study of resonance states and other continuum phenomena. By rotating the coordinates into the complex plane, the complex scaling method effectively transforms the problem into one that can be handled using standard bound state techniques.

## 2.2. Basics of scattering theory

Scattering theory is a fundamental framework in quantum mechanics used to describe and analyze the interactions between particles. At its core, it involves solving the Schrödinger equation for a system of two particles interacting via a potential. In this study, we assume the projectile has spin  $s$  and the target is in a  $0^+$  ground state. For two particles characterized by a reduced mass  $\mu$  within a specific angular momentum channel denoted by  $\alpha = \{l, s, j\}$ —where  $l$  represents the relative orbital angular momentum and  $j$  denotes the total spin of the projectile—the radial Schrödinger equation in coordinate space is expressed as follows:

$$H_\alpha(r)\psi_\alpha(r) = E\psi_\alpha(r), \quad (4)$$

where the Hamiltonian is defined as:

$$H_\alpha = -\frac{\hbar^2}{2\mu} \frac{d^2}{dr^2} + \frac{\hbar^2}{2\mu} \frac{l(l+1)}{r^2} + V_N + V_C, \quad (5)$$

with  $V_N$  representing the nuclear interaction between the projectile and the target, and  $V_C$  denoting the Coulomb potential, assuming that the nuclei are uniformly charged spheres:

$$V_C(r) = \begin{cases} \left(3 - \frac{r^2}{R_c^2}\right) \frac{z_1 z_2 e^2}{2R_c} & \text{if } r \leq R_c, \\ \frac{z_1 z_2 e^2}{r} & \text{if } r > R_c. \end{cases} \quad (6)$$

To handle the long-range nature of the Coulomb potential, we employ the “exterior complex scaling” method [22], which separates the Coulomb interaction into long-range and short-range components:

$$V_C(r) = V_C^L(r) + V_C^S(r), \quad (7)$$

where the long-range Coulomb potential, arising from the interaction between two point charges, is given by:

$$V_C^L(r) = \frac{z_1 z_2 e^2}{r}. \quad (8)$$

The solution to the Schrödinger equation exhibits asymptotic behavior described by:

$$\psi_\alpha(r) \xrightarrow{r \rightarrow \infty} F_l(\eta, kr)e^{i\sigma_l} + k f_\alpha(k)e^{i\sigma_l} O_l^{(+)}(\eta, kr), \quad (9)$$

where  $\sigma_l$  is the Coulomb phase shift,  $\eta$  is the Sommerfeld parameter,  $k$  is the wave number,  $F_l$  is the regular Coulomb function, and  $O_l^{(+)}(\eta, kr)$  denotes the Riccati-Hankel functions [23] which asymptotically behave like outgoing waves:

$$O_l^{(+)}(\eta, \rho) \xrightarrow{\rho \rightarrow \infty} e^{i\left(\rho - \frac{1}{2}l\pi - \eta \ln 2\rho + \sigma_l\right)}. \quad (10)$$

A separation of the wave function can be made as:

$$\psi_\alpha(r) = e^{i\sigma_l} F_l(\eta, kr) + \psi_\alpha^{sc}(r). \quad (11)$$

In this separation, the term  $F_l(\eta, kr)e^{i\sigma_l}$  represents the solution of the Schrödinger equation without any short-range interaction:

$$[E - T_l - V_C^L] F_l(\eta, kr) = 0, \quad (12)$$

while the second term,  $\psi_\alpha^{sc}(r)$ , is referred to as the scattered part of the wave function.

By inserting Eq. (11) into the Schrödinger equation, we obtain the inhomogeneous equation for  $\psi_\alpha^{sc}$  [1]:

$$[E - H_\alpha(r)] \psi_\alpha^{sc}(r) = e^{i\sigma_l} \tilde{V}_N F_l(\eta, kr), \quad (13)$$

where  $\tilde{V}_N$  is defined as:

$$\tilde{V}_N = V_N + V_C^S. \quad (14)$$

This quantity includes only the short-range part of the potential with both Coulomb and nuclear parts, contributing to the scattering behavior of the system.

In basic scattering theory, the scattering amplitude is expressed as:

$$f_\alpha(k) = -\frac{2\mu}{\hbar^2 k^2} e^{-i\sigma_l} \int dr F_l(\eta, kr) \tilde{V}_N(r) \psi_\alpha(r). \quad (15)$$

Upon separating the wave function, the scattering amplitude can be decomposed into two terms:

$$f_\alpha = f_\alpha^{\text{Born}} + f_\alpha^{sc}, \quad (16)$$

where the two terms are defined as:

$$f_\alpha^{\text{Born}}(k) = -\frac{1}{E} \int dr F_l(\eta, kr) \tilde{V}_N(r) F_l(\eta, kr), \quad (17)$$

and

$$f_\alpha^{sc}(k) = -\frac{1}{E} e^{-i\sigma_l} \int dr F_l(\eta, kr) \tilde{V}_N(r) \psi_\alpha^{sc}(r). \quad (18)$$

The first term,  $f_\alpha^{\text{Born}}$ , is referred to as the Born term, while the second term,  $f_\alpha^{sc}$ , represents the scattered correction to the Born term.

The colliding systems have initial and final orientations specified by the spin projections  $m_s$  and  $m'_s$  in the entrance and exit channel. The scattering amplitude for given initial and final spin projection is obtained by a sum over all channels:

$$f'_{m'_s, m_s}(\Omega) = \sqrt{4\pi} \sum_\alpha \langle l s; 0 m_s | j m_s \rangle \langle l s; m_s - m'_s, m'_s | j m_s \rangle \times \sqrt{2l+1} e^{2i\sigma_l} f_\alpha Y_l^{m_s - m'_s}(\Omega), \quad (19)$$

where  $\langle l_1 m_1; l_2 m_2 | J M_J \rangle$  is the Clebsch-Gordan coefficient,  $Y_l^m$  is the spherical harmonic function. The differential cross section for elastic scattering is determined by averaging over initial orientations and summed over final orientations:

$$\frac{d\sigma_{\text{el}}}{d\Omega} = \frac{1}{(2s+1)} \sum_{m'_s, m_s} \left| f_C(\Omega) \delta_{m'_s, m_s} + f'_{m'_s, m_s}(\Omega) \right|^2, \quad (20)$$

where the Coulomb scattering amplitude for a given scattering angle is represented by:

$$f_C(\Omega) = -\frac{\eta}{2k \sin^2\left(\frac{1}{2}\theta\right)} e^{2i\left(\sigma_0 - \eta \ln \sin\left(\frac{1}{2}\theta\right)\right)}, \quad (21)$$

<sup>1</sup> Here we only assume that the potential has a local form.

### 2.3. Application of complex scaling method to scattering theory

The complex scaling method can be applied to scattering theory to handle the scattered part of the wave function more effectively. By performing the complex scaling operation on the scattered part of the wave function, we define:

$$\psi_{\alpha}^{\text{sc},\theta}(r) = \hat{S}(\theta)\psi_{\alpha}^{\text{sc}}(r) = e^{i\theta/2}\psi_{\alpha}^{\text{sc}}(re^{i\theta}), \quad (22)$$

where  $\psi_{\alpha}^{\text{sc},\theta}(r)$  is the complex scaled scattered part of the wave function. This transformation results in an exponentially decaying asymptotic behavior of the scattered part of the wave function:

$$\psi_{\alpha}^{\text{sc},\theta}(r) \xrightarrow{r \rightarrow \infty} e^{i\theta/2} k f_{\alpha}(k) e^{-kr \sin \theta} e^{i\left(kr \cos \theta - \frac{1}{2}\pi l - \eta \ln 2kr e^{i\theta} + \sigma_l\right)}. \quad (23)$$

It can be shown that  $\psi_{\alpha}^{\text{sc},\theta}$  satisfies the following inhomogeneous equation:

$$(E - H_{\alpha}^{\theta}(r)) \psi_{\alpha}^{\text{sc},\theta}(r) = e^{i\sigma_l} e^{i\theta/2} \tilde{V}_N(re^{i\theta}) F_l(\eta, re^{i\theta}), \quad (24)$$

where the complex scaled Hamiltonian is given by:

$$H_{\alpha}^{\theta}(r) = \hat{S}(\theta) H_{\alpha} \hat{S}^{-1}(\theta) = -\frac{\hbar^2}{2\mu e^{2i\theta}} \left[ \frac{d^2}{dr^2} - \frac{l(l+1)}{r^2} \right] + V_N(re^{i\theta}) + V_C(re^{i\theta}). \quad (25)$$

Using the Cauchy theorem and the complex scaled scattered part of the wave function, correction of the scattering amplitude to the Born term can be expressed as:

$$f_{\alpha}^{\text{sc}}(k) = -\frac{2\mu}{\hbar^2 k^2} e^{i\theta/2} e^{-i\sigma_l} \int_0^{\infty} dr F_l(kre^{i\theta}) \tilde{V}_N(re^{i\theta}) \psi_{\alpha}^{\text{sc},\theta}(r). \quad (26)$$

To solve the complex-scaled Schrödinger equation (24), one can use a set of square-integrable basis functions  $\{\phi_i\}$  to expand  $\psi_{\alpha}^{\text{sc},\theta}$  as:

$$\psi_{\alpha}^{\text{sc},\theta}(r) = \sum_{i=1}^N c_i(\theta) \phi_i(r). \quad (27)$$

By substituting Equation (27) into Equation (24) and projecting onto  $\phi_i$ , a linear equation is obtained:

$$\sum_{j=1}^N \left\{ EN_{ij} - H_{l,ij}^{\theta} \right\} c_j(\theta) = b_i(\theta), \quad (28)$$

where  $N_{ij} = \langle \phi_i | \phi_j \rangle$  and the inhomogeneous term is:

$$b_i(\theta) = e^{i\theta/2} e^{i\sigma_l} \int_0^{\infty} dr \phi_i(r) \tilde{V}_N(re^{i\theta}) F_l(kre^{i\theta}), \quad (29)$$

and the matrix elements are given by:

$$H_{\alpha,ij}^{\theta} = \int_0^{\infty} \phi_i(r) H_{\alpha}^{\theta}(r) \phi_j(r) dr. \quad (30)$$

With the coefficients  $c_j(\theta)$  obtained from solving Eq. (28), the expansion can be inserted into Eq. (26), leading to the final expression for the scattered part of the scattering amplitude:

$$f_l^{\text{sc}} = -\frac{2\mu}{\hbar^2 k^2} e^{-2i\sigma_l} \sum_i c_i(\theta) b_i(\theta). \quad (31)$$

This method provides a systematic way to determine the scattering amplitude by expanding the complex scaled scattered wave function in terms of a basis set and solving the resulting linear equations.

Alternatively, using the Green's function method to solve the complex scaled Schrödinger equation, we can express the complex scaled scattered part of the wave function as:

$$\psi_{\alpha}^{\text{sc},\theta}(r) = \int dr' G_{\alpha}^{\theta}(E; r, r') \tilde{V}_N(r' e^{i\theta}) F_l(kr' e^{i\theta}). \quad (32)$$

The Green's function can be expanded as:

$$G_{\alpha}^{\theta}(E; r, r') = \sum_i \frac{\tilde{\psi}_i(r) \tilde{\psi}_i(r')}{E - \epsilon_i(\theta)}, \quad (33)$$

where  $\tilde{\psi}_i(r)$  are the eigenvectors of the complex scaled Hamiltonian:

$$H_{\alpha}(\theta) \tilde{\psi}_i(r) = \epsilon_i(\theta) \tilde{\psi}_i(r). \quad (34)$$

By combining Eq. (26), (32), and (33), a compact form of the scattering amplitude can be derived as:

$$f_{\alpha}^{\text{sc}}(k) = -\frac{2\mu}{\hbar^2 k^2} e^{i\theta} \sum_{n=1}^N \frac{d_n d_i}{E - \epsilon_i(\theta)}, \quad (35)$$

where  $d_i$  is:

$$d_i = \int dr \tilde{\psi}_i(r) V_N(re^{i\theta}) F_l(kre^{i\theta}). \quad (36)$$

This approach utilizes the Green's function to represent the complex scaled scattered wave function in terms of the eigenvectors of the complex scaled Hamiltonian, providing an alternative method to determine the scattering amplitude.

### 2.4. Optical model potential

In the study of nucleus-nucleus interactions, the Optical Model Potential (OMP) is frequently employed to describe the nuclear reactions. Here we first consider the local Optical Model Potential. The nuclear part of the Optical Model Potential consists of two parts, a partial wave independent term and a spin-orbit coupling term:

$$V_N(r) = U_N(r) + U_{so}(r). \quad (37)$$

The first term often adopts Woods-Saxon potentials and its derivatives, depending on the relative coordinate  $r$  between the nuclei:

$$U_N(r) = -V_0 \mathcal{Y}(r; R_R, a_R) - 4a_{vs} V_S \frac{d}{dr} \mathcal{Y}(r; R_{vs}, a_{vs}) - iW_0 \mathcal{Y}(r; R_W, a_W) - i4a_{ws} W_S \frac{d}{dr} \mathcal{Y}(r; R_{ws}, a_{ws}), \quad (38)$$

where the Woods-Saxon function  $\mathcal{Y}(r; R, a)$  is defined as:

$$\mathcal{Y}(r; R, a) = \frac{1}{1 + \exp((r - R)/a)}. \quad (39)$$

The spin-orbit term is defined as:

$$U_{so}(r) = 2l \cdot s V_{so} \left( \frac{\hbar}{m_{\pi} c} \right)^2 \frac{1}{r} \frac{d}{dr} \mathcal{Y}(r; R_{so}, a_{so}) + i2l \cdot s W_{so} \left( \frac{\hbar}{m_{\pi} c} \right)^2 \frac{1}{r} \frac{d}{dr} \mathcal{Y}(r; R_{so}, a_{so}). \quad (40)$$

Here,  $V_0$ ,  $W_0$ ,  $W_S$ ,  $V_S$ ,  $V_{so}$ , and  $W_{so}$  are the potential strengths, and  $R_R$ ,  $R_W$ ,  $R_{ws}$ ,  $R_{vs}$ ,  $R_{so}$ , and  $R_{so}$  are the corresponding radii, while  $a_R$ ,  $a_W$ ,  $a_{ws}$ ,  $a_{vs}$ ,  $a_{so}$ , and  $a_{so}$  are the diffuseness parameters. The scale factor for the spin-orbit term uses the mass of the pion  $m_{\pi}$  such that  $(\frac{\hbar}{m_{\pi} c})^2 \approx 2 \text{ fm}^2$ .

When extending the Woods-Saxon function into the complex plane, it exhibits a set of poles  $z_n$  given by:

$$z_n = R + i(2n + 1)\pi a, \quad n = \pm 1, \pm 2, \dots \quad (41)$$

Fig. 1 illustrates these poles on the complex plane, where the red line in the first quadrant represents the integration path when rotating the potential.

To ensure the validity of the Cauchy theorem, the contour of integration should not include these poles. This requirement imposes a restriction on the rotation angle  $\theta$ , which should satisfy:

$$\tan \theta < \frac{\pi a}{R}. \quad (42)$$

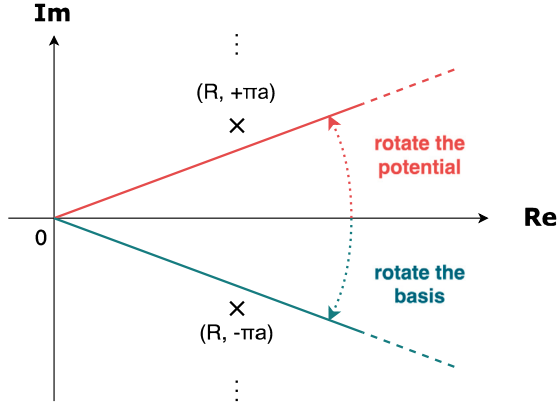


Fig. 1. Diagram illustrating the poles of the Woods-Saxon function, represented by crosses. According to the Cauchy theorem, the integration contour must exclude these poles, imposing a restriction on the rotation angle. (For interpretation of the colors in the figure(s), the reader is referred to the web version of this article.)

This restriction ensures that the contour avoids the poles of the Woods-Saxon function in the complex plane, allowing for the proper application of the complex scaling method in the calculation of the scattering amplitude with the Optical Model Potential.

By adhering to this restriction, the complex scaling method can be effectively applied to the Optical Model Potential, facilitating the analysis of scattering processes in nuclear physics. This approach ensures that the potential remains well-behaved in the complex plane, enabling accurate and reliable calculations of scattering amplitudes.

### 2.5. Perey-Buck non-local optical model

In order to further demonstrate the complex scaling method, we include the functionality to deal with non-local potentials in COLOSS. In particular, we adopt the non-local optical model potential proposed by Perey and Buck in Ref. [24], which takes the form of an ordinary optical potential multiplying with a Gaussian non-local kernel:

$$U(r, r') = U_N \left( \frac{r+r'}{2} \right) H(r-r'), \quad (43)$$

where  $U_N$  is the partial wave independent term in optical model potential defined in Eq. (38), and  $H$  is the Gaussian kernel defined as:

$$H(r-r') = \frac{\exp \left[ - \left( \frac{r-r'}{\beta} \right)^2 \right]}{\pi^{3/2} \beta^3}, \quad (44)$$

where  $\beta$  characterizes the range of non-locality. The radial Schrödinger equation with the Perey-Buck potential is rewritten as:

$$\begin{aligned} -\frac{\hbar^2}{2\mu} \left[ \frac{d^2}{dr^2} - \frac{l(l+1)}{r^2} \right] \psi_\alpha(r) + U_{so}(r) \psi_\alpha(r) + \int_0^\infty v_l(r, r') \psi_\alpha(r') dr' \\ = E \psi_\alpha(r). \end{aligned} \quad (45)$$

The Gaussian non-local kernel in Eq. (43) leads to an analytical expression of the partial wave expanded non-local potential:

$$v_l(r, r') = \frac{4rr'}{\sqrt{\pi}\beta^3} U_N \left( \frac{r+r'}{2} \right) e^{-\frac{(r^2+r'^2)}{\beta^2}} i^l j_l \left( -i \frac{2rr'}{\beta^2} \right), \quad (46)$$

where  $j_l$  is the spherical Bessel function. A similar complex scaling procedure can be carried out on Eq. (45), and the integro-differential equation can also be transformed into a set of linear equations as those defined in Eq. (28). The only difference here is that the potential matrix element should be modified as:

$$\begin{aligned} V_{ij}^\theta = e^{i\theta} \iint dr dr' \phi_i(r) v_l(r e^{i\theta}, r' e^{i\theta}) \phi_j(r') \\ + \int dr \phi_i(r) [V_C(r e^{i\theta}) + U_{so}(r e^{i\theta})] \phi_j(r), \end{aligned} \quad (47)$$

and the inhomogeneous terms should be rewritten as:

$$\begin{aligned} b_i(\theta) = e^{i\theta/2} e^{i\sigma_l} \left[ e^{i\theta} \iint_0^\infty dr dr' \phi_i(r) U_N(r e^{i\theta}, r' e^{i\theta}) F_l(kr e^{i\theta}) \right. \\ \left. + \int dr \phi_i(r) [V_C^S(r e^{i\theta}) + U_{so}(r e^{i\theta})] F_l(kr e^{i\theta}) \right]. \end{aligned} \quad (48)$$

Given that the equivalence of the linear equation method and Green's function method has been established in Ref. [19], and considering the greater computational efficiency of the linear equation method compared to eigenvalue problem-solving in practical applications, we implement only the linear equation method for addressing non-local potentials.

### 2.6. Lagrange functions and Lagrange-Laguerre basis

The Lagrange-Legendre basis is extensively employed in the  $R$ -matrix formalism [25] within nuclear physics, which is defined in the fixed interval region  $[0, 1]$ . This basis is particularly useful for problems where the wave function is confined to a finite interval, allowing for efficient and accurate numerical solutions. However, for the case of the current study, the wave function is defined in the region from 0 to  $\infty$ , making the Lagrange-Legendre basis unsuitable for use in the complex scaling method for scattering problems. The complex scaling method requires a basis that can accurately represent functions with an infinite domain, which is not possible with the Lagrange-Legendre basis.

In our numerical implementation, we utilize Lagrange-Laguerre functions regularized by  $x$  as the basis. This function, denoted by  $g_j(x)$ , is expressed as:

$$g_j(x) = (-1)^j (h_N^\alpha x_j)^{-1/2} \frac{L_N^\alpha(x)}{x-x_j} x^{\alpha/2+1} e^{-x/2}, \quad (49)$$

where  $L_N^\alpha$  represents the generalized Laguerre polynomial of order  $N$  with parameter  $\alpha$ ,  $h_N^\alpha$  corresponds to the square norms of the polynomial, and  $x_j$  are the roots of the polynomial. The generalized Laguerre polynomials  $L_N^\alpha(x)$  are orthogonal polynomials that are solutions to the Laguerre differential equation and are widely used in quantum mechanics, particularly in problems involving radial functions.

The  $x$ -regularization allows the selection of the  $\alpha$  parameter to no longer depend on  $l$  [26]. This regularization is crucial because it ensures that the basis functions have the correct asymptotic behavior at origin, which is essential for accurately representing scattering states. By decoupling the parameter  $\alpha$  from the angular momentum quantum number  $l$ , the basis functions can be tailored to better suit the specific problem at hand, providing greater flexibility and accuracy in numerical computations.

More details regarding Lagrange functions and the Lagrange-mesh method can be found in Ref. [26]. The Lagrange-mesh method is a powerful numerical technique that combines the efficiency of Gaussian quadrature with the flexibility of Lagrange interpolation. This method allows for the accurate and efficient computation of integrals and eigenvalue problems, making it highly suitable for a wide range of applications in quantum mechanics and other fields.

The  $x$ -regularized Lagrange-Laguerre functions are non-orthogonal, and the inner products between them are given by:

$$N_{ij} = \int g_i(x) g_j(x) dx = \delta_{ij} + \frac{(-1)^{i-j}}{\sqrt{x_i x_j}}. \quad (50)$$

When the order of the polynomial is large, the values of  $x_i$  may extend beyond the range of the interaction, resulting in wasted computational

effort during numerical integration. To enhance numerical efficiency, a scaling transformation is performed on the coordinate:

$$r = h_S x, \quad (51)$$

where  $h_S$  represents the scaling factor, and it has a unit of fm. The scaled basis is defined as:

$$\phi_i(r) = h_S^{-1/2} g_i(r/h_S), \quad (52)$$

where the factor  $h_S^{-1/2}$  is incorporated to maintain the same overlap  $N_{ij}$  for the scaled basis as that of the unscaled basis. Please note that both the Lagrange-Laguerre function and the variable are dimensionless. The scaling factor, which maps the Lagrange-Laguerre function and the basis function, gives the unit.

Lagrange functions are advantageous for evaluating matrix elements, especially when combined with the Gauss quadrature method. The kinetic matrix elements of the  $x$ -regularized Lagrange-Laguerre functions have an analytical form, and the non-diagonal terms can be written as

$$\begin{aligned} T_{i \neq j}^\theta &= -\frac{\hbar^2}{2\mu} \int dr \phi_i(r) \frac{d^2}{dr^2} \phi_j(r) \\ &= \frac{\hbar^2 e^{-2i\theta}}{2\mu h_S^2} \left[ \frac{(-1)^{i-j} (x_i + x_j)}{\sqrt{x_i x_j} (x_i - x_j)^2} - \frac{(-1)^{i-j}}{4\sqrt{x_i x_j}} \right], \end{aligned} \quad (53)$$

and the diagonal terms are

$$T_{ii}^\theta = -\frac{\hbar^2 e^{-2i\theta}}{2\mu h_S^2} \left\{ \frac{1}{12x_i^2} [x_i^2 - 2(2N + \alpha + 1)x_i + \alpha^2 - 4] + \frac{1}{4x_i} \right\}. \quad (54)$$

The potential matrix elements of the Lagrange functions can be expressed as:

$$V_{ij}^\theta = \int dr \phi_i(r) V(r e^{i\theta}) \phi_j(r) \approx V(r_i e^{i\theta}) \delta_{ij}. \quad (55)$$

This approximation significantly simplifies the computation process by requiring only the values of the potential at the mesh points. By focusing exclusively on these specific points, it eliminates the need to account for the interactions and behaviors of the basis functions across the entire domain.

It is important to note that, although Lagrange-Laguerre functions are very convenient to use, calculating the roots of high-order polynomials remains a numerically challenging task. This is illustrated in Fig. 2, which shows the modulus of the Laguerre function of order 40 with  $\alpha = 0$ . First, it can be observed that the modulus of the Laguerre function increases exponentially as  $x$  grows. Each drop in the graph indicates the presence of a root of the Laguerre function, where  $L_{40}^0(x) = 0$ . This means that the Laguerre function crosses the  $x$ -axis at these points, resulting in sharp drops in the modulus. However, due to numerical inaccuracies, the value does not precisely intersect with the  $x$ -axis. Moreover, as  $x$  increases, the modulus of the polynomial becomes extremely large, making the precise calculation of the roots increasingly difficult.

In certain scenarios where the approximation in Eq. (55) is not accurate enough, integration on a different mesh with more grid points may be necessary, such as on the Gauss-Legendre mesh. Instead of constructing the Lagrange-Laguerre functions from the definition provided in Eq. (49), a faster evaluation can be achieved utilizing the roots of the Laguerre polynomial. This leads to the following expression for the basis functions:

$$\phi_i(x) = \lambda_i^{-1/2} \left( \frac{r}{r_i} \right)^{\alpha/2+1} e^{-(r-r_i)/2h_S} \left( \prod_{j \neq i} \frac{r - r_j}{r_i - r_j} \right), \quad (56)$$

where  $\lambda_i$  represents the weights of the Gauss-Laguerre quadrature. This alternative approach can provide a more efficient evaluation of the basis functions and matrix elements, particularly when a higher level of accuracy is required beyond the simplified approximation.

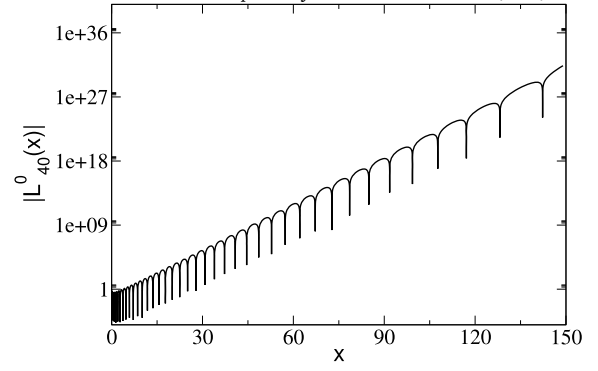


Fig. 2. Absolute value of the generalized Laguerre polynomial  $L_{40}^0(x)$ . It is shown that the polynomial oscillates rapidly when the radius becomes very large, which makes it difficult to determine the roots of the polynomial accurately.

When an analytical expression for the potential is not available, such as in cases where the potential arises from a folding procedure, direct rotation of the potential function becomes challenging. To address this, a backward rotation can be introduced to the basis functions. Assuming that only discrete values for the potential are available on specific mesh points along the real axis, the integral can be transformed using the Cauchy theorem as follows:

$$V_{ij}(\theta) = e^{-i\theta} \int_0^\infty \phi_i(re^{-i\theta}) V(r) \phi_j(re^{-i\theta}) dr. \quad (57)$$

This transformation allows for the evaluation of the potential using values solely at particular mesh points along the real axis. It is important to note that after rotating the basis backwards, the approximation in Eq. (55) is no longer valid. Therefore, all matrix elements must be evaluated using the Gauss quadrature method.

Similarly, the inhomogeneous terms in Eq. (24) can also be transformed in a similar manner:

$$b_i(\theta) = e^{-i\theta/2} e^{i\sigma_i} \int_0^\infty dr \phi_i(re^{-i\theta}) \tilde{V}_N(r) F_l(kr). \quad (58)$$

By employing these transformations, it becomes feasible to handle situations where the potential is not analytically defined, enabling the evaluation of matrix elements and inhomogeneous terms with discrete potential values on specific mesh points along the real axis. The rotation on the basis is shown in the fourth quadrant of Fig. 1 with green lines. Although here the basis functions do not have poles, the restriction still exists to make the Cauchy theorem valid when calculating the scattering amplitude according to Eq. (26). With this back rotation technique, we implement the feature that allows users to import any central potential from an external file.

### 3. Program description

#### 3.1. Input description

We use the namelist feature in our programming to construct the input of the program into groups of variables, making it more readable and easier to use. By organizing variables into logical groups, the namelist enhances the clarity and maintainability of the code, facilitating easier debugging and modification. The following is a detailed description of the namelist:

##### 1. General Namelist

- nr (integer\*4): Number of the Lagrange-Laguerre basis used in the calculation.
- alpha (real\*8):  $\alpha$  parameter of the Laguerre polynomial in Eq. (49).

- `Rmax` (real\*8): Maximum value of the points in the scaled Lagrange-Laguerre mesh, which satisfies:

$$R_{\max} = h_s x_{\max} \quad (59)$$

- `ctheta` (real\*8): rotation angle for complex scaling in degrees.
- `cwftype` (integer\*4): type of the subroutines called in the program to calculate Coulomb wave functions: 1 for `COULCC` and 2 for `cwfcomplex`.
- `matgauss` (logical): boolean variable which determines whether to use the Gauss-Legendre quadrature to evaluate the matrix elements.
- `bgauss` (logical): boolean variable which determines whether to use the Gauss-Legendre quadrature to evaluate the inhomogeneous terms in the linear equation.
- `backrot` (logical): boolean variable controls the method used for the evaluation of potential matrix elements. If set to `.TRUE.`, the basis will undergo a backward rotation, and the potential matrix elements will be computed according to eq. (57). If set to `.FALSE.`, the potential will be directly rotated, and the matrix elements will be computed following eq. (30). Make sure that `matgauss` and `bgauss` are `.TRUE.` before setting `backrot` as `.TRUE.`
- `numgauss` (integer\*4): number of Gauss-Legendre mesh points used in the evaluation of the matrix elements.
- `rmxgauss` (real\*8): maximum radius of the Gauss-Legendre mesh points.
- `method` (integer\*4): option for two different methods to calculate the scattering amplitude. Set it as 1 for linear equation method, and 2 for the Green's function method.
- `thetastep` (real\*8): step size for the angle in the output differential cross section.
- `thetamax` (real\*8): maximum value of the angle in the output differential cross section.
- `readinpot` (logical): boolean variable controls whether to read the potential from external file 'pot.dat'.

## 2. System Namelist

- `zp`, `massp` (real\*8): charge and mass number of the projectile.
- `zt`, `masst` (real\*8): charge and mass number of the target.
- `jmin/jmax` (integer\*4): minimum/maximum total angular momentum of the reaction system considered in the calculation.
- `sp` (real\*8): spin of the projectile.
- `elab` (real\*8): incident kinetic energy of the projectile in the laboratory frame.

## 3. Pot Namelist

- `vv`, `rv`, `av` (real\*8): depth, radius, and width parameters of the real volume term in optical model potential (OMP).
- `wv`, `rw`, `aw` (real\*8): depth, radius, and width parameters of the imaginary volume term in OMP.
- `vs`, `rvs`, `avs` (real\*8): depth, radius, and width parameters of the real surface term in OMP.
- `ws`, `rws`, `aws` (real\*8): depth, radius, and width parameters of the imaginary surface term in OMP.
- `vsov`, `rsov`, `asov` (real\*8): depth, radius, and width parameters of the real spin-orbit coupling term in OMP.
- `vsow`, `rsow`, `asow` (real\*8): depth, radius, and width parameters of the imaginary spin-orbit coupling term in OMP.
- `rc` (real\*8): charge radius for Coulomb interaction in OMP.

## 4. nonlocalpot Namelist

- `nonlocal` (logical): boolean variable which determines whether to use the non-local form of optical potential introduced in Ref. [24]. Please set `method=1` to use linear equation method to deal with non-local potentials, and set `bgauss=t` for a higher precision of the potential matrix.

- `nlbeta` (real\*8): parameter  $\beta$  in the Gaussian non-local kernel defined in eq. (44).

## 3.2. Output description

1. The local copy of the input file is stored in `fort.1`.
2. The list for all the angular momentum channels considered in the calculation is stored in `fort.2`
3. The scaled Lagrange-Laguerre mesh points and weights are stored in `fort.10`.
4. The  $S$ -matrices for different angular momentum channels are stored in `fort.60`.
5. The nuclear scattering amplitudes for different angular momentum channels are stored in `fort.61`.
6. The angular distribution of the differential cross section is stored in `fort.67`.

## 3.3. Read the potential from an external file

We have implemented a feature that allows users to import any central potential from an external file for calculations. This implementation is similar to that of Fresco [27]. To utilize this feature, set `readinpot` to `.TRUE.` and employ the back rotation method. The potential file should be named 'pot.dat' and must include a header with specific formatting: the first line should contain a descriptive string, the second line should list the number of potential points, the step size of the radius, and the starting radius point. Subsequent lines should detail the real and imaginary parts of the potential. An example is as follows:

```
pot_data_for_alpha+40Ca
1201 0.05 0
-46.441365838950894      -1.7807234710243705
-46.432765180897832      -1.7811723376269695
.....
```

## 3.4. Structure of the main program and the workflow

The main program consists of some important subroutines, and the following is a detailed explanation of their functionalities:

- `read_input`: Reads the input variables through the Fortran namelist.
- `init_laguerre_mesh`: Initializes the abscissas and weights of the Lagrange-Laguerre mesh and performs the scale transformation.
- `get_pot_para`: Initializes the parameters of the optical potential.
- `lagrange_function`: Generates the Lagrange-Laguerre basis on the Gauss-Legendre mesh.
- `initial_coul`: Generates the Coulomb wave functions on the rotated coordinate and the original coordinate.
- `solve_scatt`: Generates the Hamiltonian matrix, solves the linear equation, gets the complex scaled wave function, and calculates the scattering amplitudes.
- `solve_bound`: Generates the Hamiltonian matrix, solves the eigenvalue problem, and gets the eigenvalues and the eigenvectors.
- `solve_scatt_green`: Uses the eigenvalues and the eigenvectors to expand the Green's operator, and calculates the scattering amplitudes.
- `xsec`: The scattering amplitudes are used to calculate the angular distribution of the differential cross section.

Fig. 3 provides a detailed overview of the workflow within the primary segment of the program. The bold text within the figure denotes the names of the subroutines employed in the program, whereas the regular text offers concise explanations of these subroutines along with their corresponding formulas in the paper. The left segment of the figure delineates the workflow for the linear equation method. Initially, the

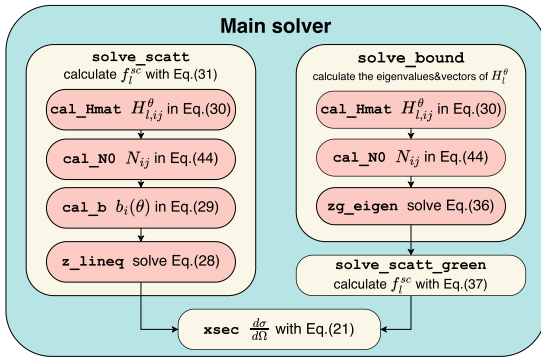


Fig. 3. Workflow of the COLOSS program. See text for more details.

matrix elements of the Hamiltonian are computed according to Eq. (30). Subsequently, the inner product of the basis is generated following Eq. (50). Finally, the linear equation specified in Eq. (28) is resolved, leading to the calculation of the scattered component of the scattering amplitude in accordance with Eq. (31). Conversely, the right segment of the figure illustrates the workflow for the Green's function method. Analogous to the linear equation method, the matrix elements of the Hamiltonian and the inner product matrix are initially computed. Next, the eigenvalue problem detailed in Eq. (34) is solved, yielding the eigenvalues and eigenvectors. These eigenvalues and eigenvectors are then utilized to expand the Green's function through Eq. (33), subsequently enabling the calculation of the scattered part of the scattering amplitude via Eq. (35). By leveraging the scattered part of the scattering amplitude derived from two methods, the angular distribution of the differential cross-section is finally computed following Eq. (20).

### 3.5. List of additional subroutines

In addition to the main subroutines, the program incorporates several other open-source subroutines. Below is a brief description of these subroutines:

1. `COULCC`: This subroutine calculates the Coulomb wave function for complex arguments  $\rho$ ,  $\eta$ , and  $l$  [28].
2. `cfcomplex`: It is used to compute the Coulomb wave function for a broader range of complex arguments  $\rho$ ,  $\eta$ , and  $l$ . The original code was written in C++ by N. Michel [29], and an interface is provided here to allow Fortran to call it.
3. `cdgqf`: This subroutine computes the Gauss quadrature abscissas and weights [30]. In this subroutine, it is specifically used to generate the Lagrange-Laguerre mesh.
4. `PLM`: It calculates the associated Legendre polynomial. This subroutine is sourced from FRESKO [27].

## 4. Examples

### 4.1. Installation and compilation

We provide illustrative examples demonstrating the execution of the program under a range of conditions. All examples have been tested on a DELL PowerEdge T640 Tower Server equipped with an Ubuntu 20.04.3 LTS operating system. The server features an Intel(R) Xeon(R) Gold 6248R CPU running at 3.00 GHz and is equipped with 640 GB of memory. A concise guide to execute the code is outlined below:

1. We provide a Makefile to help compile and link all the codes. Ensure proper linkage with LAPACK by specifying the LAPACK path on your local machine in the LIB variable within the provided Makefile:  
LIB = -L/path/of/your/local/lapack -llapack

Table 1

Computing time comparison of COLOSS and Numerov. Both programs are executed for 100 times, and the average computing time for each run is computed.

Method	Numerov	COLOSS
avg. time ( $10^{-2}$ s)	4.430	2.353

2. In COLOSS, we use gFortran as our Fortran compiler and GCC to bind the C++ code with our Fortran code. Please make sure that GCC is installed on your machine. One can compile the program with the provided Makefile by executing:

```
> make
```

3. Transfer the executable program, COLOSS, to the test directory, and initiate program execution through standard input:

```
> ./COLOSS < inputfile
```

### 4.2. Example 1: neutron + $^{40}\text{Ca}$ scattering

We first present a simple case for neutron +  $^{40}\text{Ca}$  scattering without Coulomb interaction. The neutron-nucleus interaction is taken from the Koning-Delaroche (KD) parameterization [31]. In this example, we take advantage of the Lagrange functions and use Eq. (55) to evaluate all the matrix elements and the inhomogeneous terms in Eq. (28). Consequently, the potential matrix is rendered diagonal, simplifying the computational process to merely requiring the potential values at mesh points. To make a comparison of our method, we also use the Numerov method implemented in FRESKO [27] to calculate the cross section.

The input file for the linear equation method is as follows:

```
&general
  nr=60  alpha=0  Rmax=40  ctheta=5
  matgauss=f  bgauss=f  method=1
  thetah=1.0  thetamax=180 /

&system
  zp=0  massp=1  namep='n'
  zt=20  masst=40  namet='40Ca'
  jmin=0  jmax=10  elab=20  sp=0.5/

&pot
  vv=46.553  rv=1.185  av=0.672
  vw=1.777  rw=1.185  aw=0.672
  vs=0  rvs=0  avs=0
  ws=7.182  rws=1.288  aws=0.538
  vsov=5.343  rsov=0.996  asov=0.590
  vsow=-0.110  rsow=0.996  asow=0.590
  rc=1.698 /

&non-local_pot
  non-local=f  non-local_beta=0.0 /
```

The angular distribution of the cross section is illustrated in Fig. 4. In this figure, the black solid line represents the result obtained using the Numerov method, the red dashed line depicts the result from COLOSS using the linear equation method. Notably, the complete overlap of these two lines serves as a robust validation of the accuracy of the complex scaling method employed in our analysis. For the performance test, we executed the program 100 times and calculated the average time for each run. The comparative computing times between COLOSS and Numerov methods in this example are presented in Table 1.

In the Numerov calculation, the matching radius is set at 40 fm, consistent with Rmax in COLOSS, and the step size for the radial integration is 0.05 fm. It is important to note that Fresco is not specifically designed to address the same problems as our code, and it includes many additional functionalities and outputs. Therefore, making an absolutely fair

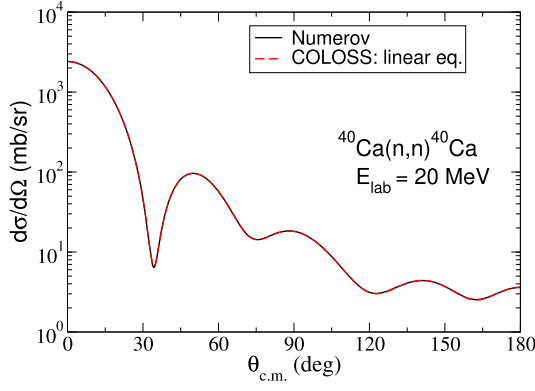


**Fig. 4.** Cross section for neutron +  $^{40}\text{Ca}$  elastic scattering at the incident energy of 20 MeV for neutron in the laboratory frame. The black solid line represents the result from Numerov, the red dashed line represents the result given by COLOSS with the linear equation method.

comparison is challenging. Nonetheless, we hope these comparisons will provide a basic indication of our program's performance.

#### 4.3. Example 2: deuteron + $^{93}\text{Nb}$ scattering

Here we present the second example to calculate the deuteron +  $^{93}\text{Nb}$  scattering at 20 MeV for deuteron. For the deuteron-nucleus interaction, we adopt the parameters from Ref. [32]. We include the results of both the linear equation method and the Green's function method for comparison.

The input file for the linear equation method is as follows:

```
&general
nr=60 alpha=0 Rmax=40 ctheta=6
matgauss=f bgauss=f method=2
thetah=1.0 thetamax=180 /

&system
zp=1 massp=2 namep='2H'
zt=41 masst=93 namet='93Nb'
jmin=0 jmax=20 elab=20 sp=1.0/

&pot
vv=84.323 rv=1.174 av=0.809
wv=0.351 rw=1.563 aw=0.904
vs=0 rvs=0 avs=0
ws=14.247 rws=1.328 aws=0.669
vsov=3.703 rsov=1.234 asov=0.813
vsow=-0.206 rsow=1.234 asow=0.813
rc=1.698 /

&non-localpot
non-local=f nlbeta=0.0 /.
```

For the calculation with the Green's function method, please change method to 2.

The angular distribution of the cross section is illustrated in Fig. 5. In this figure, the black solid line represents the result obtained using the Numerov method, the red dashed line depicts the outcome from COLOSS using the linear equation method, and the green dotted line shows the result from COLOSS employing the Green's function method.

The results exhibit a remarkable agreement among the three methods, indicating that complex scaling can be effectively utilized with the realistic optical model potentials. This concurrence also highlights the precision of the approximation described in Eq. (55). However, it is important to note that solving an eigenvalue problem is significantly more

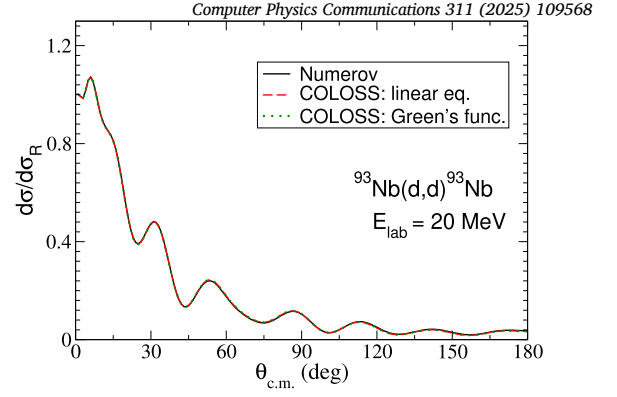


**Fig. 5.** Cross section for deuteron +  $^{93}\text{Nb}$  elastic scattering at the incident energy of 20 MeV for deuteron in the laboratory frame. The black solid line represents the result from Numerov, the red dashed line represents the result given by COLOSS with the linear equation method, and the green dotted line represents the result given by COLOSS with the Green's function method.

**Table 2**

Computing time comparison between linear equation method, Green's function method in COLOSS and Numerov method.

Method	Numerov	Linear eq.	Green's func.
avg. time( $10^{-2}$ s)	7.77	6.31	68.44

time-consuming compared to solving a linear equation. Consequently, the linear equation method emerges as a more practical option. The inclusion of the Green's function method serves to demonstrate the numerical equivalence between these two approaches. The performance test was also conducted by averaging the computing times over 100 runs, and the computing times for the three methods are listed in Table 2.

In the Numerov calculation, the matching radius is set at 40 fm, identical to Rmax in COLOSS, with a step size of 0.05 fm for the radial integration. It is observed that the Green's function method is significantly slower than both the Numerov and the linear equation methods. This discrepancy is primarily due to the fact that solving an eigenvalue problem is considerably more computationally expensive than solving a linear equation.

#### 4.4. Example 3: $\alpha$ + $^{28}\text{Si}$ scattering

The third example involves  $\alpha$  +  $^{28}\text{Si}$  scattering at an incident energy of 30 MeV for the  $\alpha$  particle. The  $\alpha$ -nucleus interaction parameters are sourced from Ref. [33]. In this example, both the approximation for Lagrange functions in Eq. (55) and the direct Gauss-Legendre quadrature method are employed to evaluate the matrix element.

The input file for the calculation using the direct Gauss-Legendre quadrature method is as follows:

```
&general
nr=100 alpha=0 Rmax=50 ctheta=6
matgauss=t bgauss=t
numgauss=300 rmaxgauss=100
thetah=1.0 thetamax=180 /

&system
zp=2 massp=4 namep='4He'
zt=14 masst=28 namet='28Si'
jmin=0 jmax=20 elab=30 /

&pot input_pot_type=1
vv=155.832 rv=1.342 av=0.658
wv=0.210 rw=1.426 aw=0.559
```

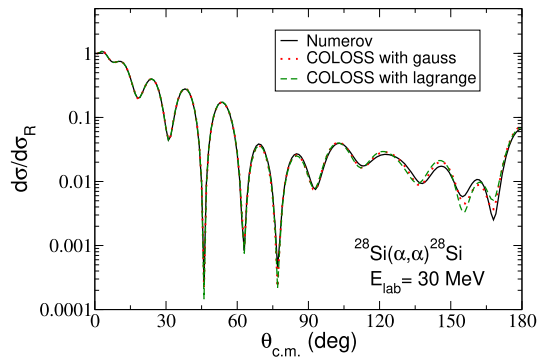


**Fig. 6.** Cross section for  $\alpha + {}^{28}\text{Si}$  elastic scattering at an incident energy of 30 MeV for the  $\alpha$  particle in the laboratory frame. The black solid line represents the result from Numerov, the red dotted line represents the result from COLOSS using Gauss-Legendre quadrature, and the green dashed line represents the result from COLOSS using the Lagrange approximation.

**Table 3**

Values of  $S$ -matrices for different angular momenta with different integration methods. The results of Numerov are included for comparison. See text for more details.

$S_l$	Numerov	Approx.	Exact
$l = 11$	(0.2230,0.0810)	(0.222,0.081)	(0.2227,0.0808)
$l = 12$	(0.4020,0.2203)	(0.401,0.220)	(0.4019,0.2203)
$l = 13$	(0.6897,0.2595)	(0.689,0.259)	(0.6897,0.2596)
$l = 14$	(0.8773,0.1713)	(0.8773,0.1713)	(0.8773,0.1713)
$l = 15$	(0.9512,0.0907)	(0.9512,0.0907)	(0.9512,0.0907)

```
vs=0 rvs=0 avs=0
ws=25.191 rws=1.293 aws=0.636
rc=1.35/
```

```
&non-localpot
non-local=f nlbeta=0.0 /.
```

To perform the approximated calculation, one can set `matgauss` and `bgauss` to `.FALSE.`. The angular distribution of the cross section is depicted in Fig. 6. In this figure, the black solid line represents the result from Numerov, the red dotted line represents the result from COLOSS using Gauss-Legendre quadrature, and the green dashed line represents the result from COLOSS using the Lagrange approximation.

It is important to note that the complex-scaled Hamiltonian matrix with Lagrange-Laguerre functions is typically non-diagonal. This example aims to compare the results generated by an approximated diagonal Hamiltonian matrix with those produced by the exact non-diagonal counterpart. The figure shows that there is only a slight difference between the red dotted line and the green dashed line. Notably, for large scattering angles, the line representing the exact results is closer to the line produced by Numerov.

To compare the results of the two different integration methods in detail, we provide a table of the  $S$ -matrices for selected angular momenta. The results are shown in Table 3. The results generated with the approximation in Eq. (55) are labeled “Approx.,” and the results generated with the direct Gauss-Legendre quadrature are labeled “Exact”. For the calculation, `Rmax` is set to 50 fm, and the rotation angle is set to 6 degrees. By increasing the number of basis functions up to 100, all the converged digits are displayed in the table.

Upon close examination of the results, it becomes evident that the discrepancies among the three outcomes are minimal. However, a notable distinction lies in the slower convergence rate observed for the approximation method. To elucidate this phenomenon, we provide a detailed comparison focusing on the convergence behavior of the two integration methods. This analysis is systematically presented in Table 4. Specifically, we examine  $S_{l=11}$  across varying numbers of basis functions.

The comparative analysis distinctly demonstrates that the Gauss-Legendre quadrature method achieves convergence at a significantly faster rate than the approximation method. The underlying reason for this discrepancy can be attributed to the challenges associated with accurately calculating the roots of Laguerre polynomials, as depicted in Fig. 2. As previously discussed, increasing the number of basis functions inherently introduces new errors when employing Eq. (55) for matrix element evaluation. Conversely, the Gauss-Legendre quadrature method does not encounter such issues, owing to its inherent numerical stability and accuracy. Given these observations, it is advisable to utilize the Gauss-Legendre quadrature over the approximation method described in Eq. (55), particularly when dealing with a large number of basis functions.

#### 4.5. Example 4: ${}^6\text{Li} + {}^{208}\text{Pb}$ scattering

The fourth example involves  ${}^6\text{Li} + {}^{208}\text{Pb}$  scattering at an incident energy of 40 MeV for  ${}^6\text{Li}$ . This reaction, which includes a heavy nucleus with strong Coulomb interaction, is considered at near-barrier energy. When the Sommerfeld parameter is very large, the more recently developed code by N. Michel offers enhanced numerical stability for calculating the Coulomb functions with complex arguments. Therefore, in this example, the `cfComplex` code is utilized to compute all Coulomb wave functions through an interface between Fortran and C++. Additionally, we present two different rotation methods mentioned in the previous chapter: the first is to rotate the interaction, and the second is to rotate the basis, as shown in Eq. (57). This allows us to confirm the numerical self-consistency for different rotation methods and provide solutions when an analytical expression for the potential is not available.

The input file for rotating the potential is as follows:

```
&general
nr=100 alpha=0 Rmax=40 ctheta=4
matgauss=t bgauss=t
numgauss = 400 rmaxgauss=150
thetah=0.5 thetamax=180
cwftype=2 backrot=f/

&system
zp=3 massp=6 namep='6Li'
zt=82 masst=208 namet='208Pb'
jmin=0 jmax=40 elab=40 /

&pot input_pot_type=1
vv=109.500 rv=1.326 av=0.811
wv=22.384 rw=1.534 aw=0.884
vs=0 rvs=0 avs=0
ws=0 rws=0 aws=0
rc=1.3 /

&non-localpot
non-local=f nlbeta=0.0 /.
```

To rotate the basis function, set `backrot` to `.TRUE.`. It should be noted that, since the approximation in Eq. (55) cannot be applied to the rotated basis, both `matgauss` and `bgauss` must be set to `.TRUE.` before setting `backrot` to `.TRUE.`. The angular distribution of the cross section is shown in Fig. 7. In this figure, the black solid line represents the result from Numerov, the red dashed line represents the result given by COLOSS with rotation on the potential, and the green dashed line represents the result given by COLOSS with rotation on the basis. According to the figure, these three lines almost overlap, confirming the numerical self-consistency of the two different rotation methods and the accuracy of these methods compared to Numerov.

**Table 4**

Convergence test of the approximation for Lagrange functions. See text for more details.

$S_{11}$	NR=40	NR=60	NR=80	NR=100
Approx.	(0.2544,0.1053)	(0.2235,0.0810)	(0.2224,0.0813)	(0.2225,0.0810)
Exact	(0.2237,0.0804)	(0.2227,0.0807)	(0.2227,0.0807)	(0.2227,0.0807)

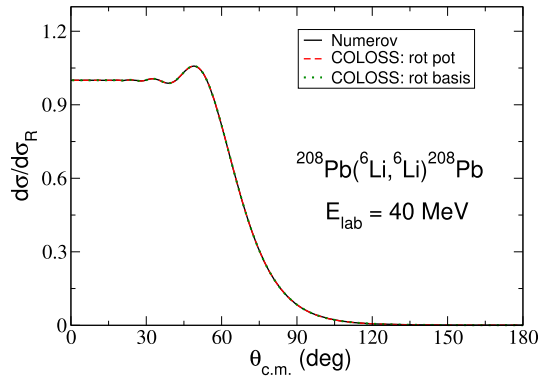


**Fig. 7.** Cross section for  ${}^6\text{Li} + {}^{208}\text{Pb}$  elastic scattering at an incident energy of 40 MeV for  ${}^6\text{Li}$  in the laboratory frame. The black solid line represents the result from Numerov, the red dashed line represents the result given by COLOSS with rotation on the potential, and the green dashed line represents the result given by COLOSS with rotation on the basis.

#### 4.6. Example 5: neutron + ${}^{56}\text{Fe}$ scattering with a non-local potential

In the last example, we consider the elastic scattering between neutron and  ${}^{56}\text{Fe}$ , where we adopt the Perey-Buck non-local form of optical model potential [24]. This example primarily serves as a benchmark to assess the effectiveness of the complex scaling method in addressing non-local potentials. It is not intended for direct comparison with experimental data. For the comparative calculations, we employ the  $R$ -matrix package developed by P. Descouvemont [34].

For the calculation of non-local potentials, please set `non-local` as `.TRUE.` and choose a proper value for the non-local range parameter  $\beta$ . The input file is as follows:

```
&general
nr=50 alpha=0 Rmax=40 ctheta=7
matgauss=t bgauss=t method=1
backrot=t
numgauss = 100 rmaxgauss=70
thetah=1.0 thetamax=180 /

&system
zp=0 massp=1 namep='n'
zt=26 masst=56 namet='56Fe'
jmin=0 jmax=12 elab=15.0 sp=0.5/

&pot
vv=53.662 rv=1.198 av=0.669
wv=0 rw=1.198 aw=0.669
vs=0 rvs=0 avs=0
ws=8.310 rws=1.282 aws=0.548
vsov=5.343 rsov=0.996 asov=0.590
vsow=-0.110 rsow=0.996 asow=0.590
rc=1.26 /

&non-localpot
non-local=t nlbeta=2.0 /
```

The angular distribution of the cross section in this example is illustrated in Fig. 8. In this figure, the black solid line represents the result

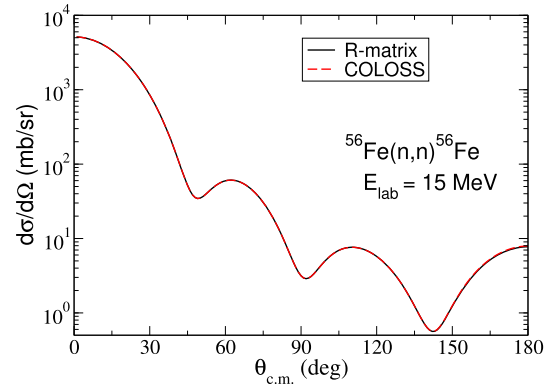


**Fig. 8.** Cross section for  $n + {}^{56}\text{Fe}$  elastic scattering at an incident energy of 15 MeV for neutron in the laboratory frame. The black solid line represents the result from  $R$ -matrix calculation, the red dashed line represents the result given by COLOSS with rotation on the basis functions through the linear equation method.  $R$ -matrix calculation is performed with the package developed by P. Descouvemont [34].

obtained using the  $R$ -matrix method, the red dashed line depicts the outcome from COLOSS with rotation on the basis functions using the linear equation method. It is evident from the results that there is a complete overlap between the two methods, demonstrating the high accuracy achievable when incorporating non-local potentials into the complex scaling method. Compared to direct integration methods such as Numerov, the basis expansion approach within the complex scaling framework offers a more convenient means of handling non-local potentials.

## 5. Conclusion

In this study, we introduced a program designed to calculate elastic scattering between two nuclei with the general local optical model potential and the Perey-Buck non-local optical potential, leveraging the complex scaling method. Our program features a user-friendly input format, enabling users to adjust and utilize various parameters of the optical model potential. By applying the complex scaling method, the scattered part of the wave function transitions from an oscillatory form to an exponentially decaying one. This transformation in the asymptotic behavior obviates the necessity of imposing boundary conditions in the solution, allowing us to expand the wave function using a complete set of square-integrable basis functions.

In evaluating the matrix element of the complex-scaled Hamiltonian, we began by conducting a thorough analysis of the analytic properties of the Woods-Saxon function on the complex plane. We clarified the constraints imposed on the rotation angle by the Cauchy theorem. Subsequently, we introduced two distinct methods for numerical integration along with two rotation techniques. These technical discussions aim to enhance our understanding of the validity of the complex scaling method and the appropriateness of the chosen basis functions.

Finally, we demonstrated the program through three examples that showcase its functionality under various conditions. Each example emphasized a particular numerical aspect discussed in the paper, and we provided results obtained by Numerov for comparative analysis. The outcomes of these examples demonstrated robust agreement with Numerov's results, underscoring the program's high accuracy, the effectiveness of the complex scaling method for the optical model potential, and

the numerical consistency of the program. Consequently, this program emerges as a valuable tool for applying the complex scaling method in continuum states calculations, particularly for computing elastic scattering between two nuclei.

The development of this program opens up the possibility to study more complicated problems, such as solving the inclusive breakup within the framework of quantum three-body problems. This extension would further enhance the program's applicability and contribute significantly to the field of nuclear physics.

### CRedit authorship contribution statement

**Junzhe Liu:** Writing – original draft, Software, Methodology, Investigation, Formal analysis. **Jin Lei:** Writing – review & editing, Supervision, Project administration, Methodology, Funding acquisition, Conceptualization. **Zhongzhou Ren:** Writing – review & editing, Project administration, Funding acquisition.

### Declaration of competing interest

The authors declare that they have no known competing financial interests or personal relationships that could have appeared to influence the work reported in this paper.

### Acknowledgements

We are grateful to Rimantas Lazauskas for his guidance in implementing the complex scaling method. This work has been supported by the National Natural Science Foundation of China (Grants No. 12475132, No.12105204, and No.12035011), by the National Key R&D Program of China (Contract No. 2023YFA1606503), and by the Fundamental Research Funds for the Central Universities.

### Data availability

No data was used for the research described in the article.

### References

- [1] A.B. Balantekin, J. Carlson, D.J. Dean, G.M. Fuller, R.J. Furnstahl, M. Hjorth-Jensen, R.V.F. Janssens, B.-A. Li, W. Nazarewicz, F.M. Nunes, W.E. Ormand, S. Reddy, B.M. Sherrill, Nuclear theory and science of the facility for rare isotope beams, *Mod. Phys. Lett. A* 29 (11) (2014) 1430010, <https://doi.org/10.1142/S0217732314300109>.
- [2] J.E. Escher, J.T. Harke, F.S. Dietrich, N.D. Scielzo, I.J. Thompson, W. Younes, Compound-nuclear reaction cross sections from surrogate measurements, *Rev. Mod. Phys.* 84 (2012) 353–397, <https://doi.org/10.1103/RevModPhys.84.353>, <https://link.aps.org/doi/10.1103/RevModPhys.84.353>.
- [3] E.P. Wigner, Resonance reactions and anomalous scattering, *Phys. Rev.* 70 (1946) 15–33, <https://doi.org/10.1103/PhysRev.70.15>, <https://link.aps.org/doi/10.1103/PhysRev.70.15>.
- [4] E.P. Wigner, Resonance reactions, *Phys. Rev.* 70 (1946) 606–618, <https://doi.org/10.1103/PhysRev.70.606>, <https://link.aps.org/doi/10.1103/PhysRev.70.606>.
- [5] A. La Piana, W. Leidemann, Calculation of exclusive cross sections with the Lorentz integral transform method, *Nucl. Phys. A* 677 (1) (2000) 423–441, [https://doi.org/10.1016/S0375-9474\(00\)00310-9](https://doi.org/10.1016/S0375-9474(00)00310-9), <https://www.sciencedirect.com/science/article/pii/S0375947400003109>.
- [6] F.A. McDonald, J. Nuttall, Complex-energy method for elastic e-h scattering above the ionization threshold, *Phys. Rev. Lett.* 23 (1969) 361–363, <https://doi.org/10.1103/PhysRevLett.23.361>, <https://link.aps.org/doi/10.1103/PhysRevLett.23.361>.
- [7] F.A. McDonald, J. Nuttall, Further calculations of s-wave elastic e – H scattering above the ionization threshold by the complex-energy method, *Phys. Rev. A* 4 (1971) 1821–1824, <https://doi.org/10.1103/PhysRevA.4.1821>, <https://link.aps.org/doi/10.1103/PhysRevA.4.1821>.
- [8] T. Myo, K. Katō, S. Aoyama, K. Ikeda, Analysis of <sup>6</sup>He Coulomb breakup in the complex scaling method, *Phys. Rev. C* 63 (2001) 054313, <https://doi.org/10.1103/PhysRevC.63.054313>, <https://link.aps.org/doi/10.1103/PhysRevC.63.054313>.
- [9] R. Lazauskas, J. Carbonell, Application of the complex-scaling method to few-body scattering, *Phys. Rev. C* 84 (2011) 034002, <https://doi.org/10.1103/PhysRevC.84.034002>, <https://link.aps.org/doi/10.1103/PhysRevC.84.034002>.
- [10] J. Carbonell, A. Deluva, A. Fonseca, R. Lazauskas, Bound state techniques to solve the multiparticle scattering problem, *Prog. Part. Nucl. Phys.* 74 (2014) 55–80, <https://doi.org/10.1016/j.pnpnp.2013.10.003>, <https://www.sciencedirect.com/science/article/pii/S0146641013000938>.
- [11] R. Hartree, J.G.L. Michel, P. Nicolson, Meteorological factors in radiowave propagation, in: *Report of a Conference held on 8th April 1946 at The Royal Institution, London by The Physical Society and The Royal Meteorological Society, The Physical Society, London, 1946*, pp. 127–168.
- [12] J. Nuttall, H.L. Cohen, Method of complex coordinates for three-body calculations above the breakup threshold, *Phys. Rev.* 188 (1969) 1542–1544, <https://doi.org/10.1103/PhysRev.188.1542>, <https://link.aps.org/doi/10.1103/PhysRev.188.1542>.
- [13] Y. Ho, The method of complex coordinate rotation and its applications to atomic collision processes, *Phys. Rep.* 99 (1) (1983) 1–68, [https://doi.org/10.1016/0370-1573\(83\)90112-6](https://doi.org/10.1016/0370-1573(83)90112-6), <https://www.sciencedirect.com/science/article/pii/0370157383901126>.
- [14] N. Moiseyev, Quantum theory of resonances: calculating energies, widths and cross-sections by complex scaling, *Phys. Rep.* 302 (5) (1998) 212–293, [https://doi.org/10.1016/S0370-1573\(98\)00002-7](https://doi.org/10.1016/S0370-1573(98)00002-7), <https://www.sciencedirect.com/science/article/pii/S0370157398000027>.
- [15] A.T. Kruppa, R.G. Lovas, B. Gyarmati, Complex scaling in the cluster model: resonances in <sup>8</sup>Be, *Phys. Rev. C* 37 (1988) 383–389, <https://doi.org/10.1103/PhysRevC.37.383>, <https://link.aps.org/doi/10.1103/PhysRevC.37.383>.
- [16] C. Kurokawa, K. Katō, New broad 0<sup>+</sup> state in <sup>12</sup>C, *Phys. Rev. C* 71 (2005) 021301, <https://doi.org/10.1103/PhysRevC.71.021301>, <https://link.aps.org/doi/10.1103/PhysRevC.71.021301>.
- [17] R.T. Baume, M.C. Crocker, J. Nuttall, Limitations of the method of complex basis functions, *Phys. Rev. A* 12 (1975) 486–492, <https://doi.org/10.1103/PhysRevA.12.486>, <https://link.aps.org/doi/10.1103/PhysRevA.12.486>.
- [18] B.R. Johnson, W.P. Reinhardt, Observation of Padé summability in divergent L<sup>2</sup> complex coordinate calculations of t-matrix amplitudes in the presence of long-range forces, *Phys. Rev. A* 29 (1984) 2933–2935, <https://doi.org/10.1103/PhysRevA.29.2933>, <https://link.aps.org/doi/10.1103/PhysRevA.29.2933>.
- [19] A.T. Kruppa, R. Suzuki, K. Katō, Scattering amplitude without an explicit enforcement of boundary conditions, *Phys. Rev. C* 75 (2007) 044602, <https://doi.org/10.1103/PhysRevC.75.044602>, <https://link.aps.org/doi/10.1103/PhysRevC.75.044602>.
- [20] J. Liu, J. Lei, Z. Ren, A complex scaling method for efficient and accurate scattering emulation in nuclear reactions, *Phys. Lett. B* 858 (2024) 139070, <https://doi.org/10.1016/j.physletb.2024.139070>, <https://www.sciencedirect.com/science/article/pii/S0370269324006282>.
- [21] N. Moiseyev, *Non-Hermitian Quantum Mechanics*, Cambridge University Press, 2011.
- [22] M.V. Volkov, N. Elander, E. Yarevsky, S.L. Yakovlev, Solving the Coulomb scattering problem using the complex-scaling method, *Europhys. Lett.* 85 (3) (2009) 30001, <https://doi.org/10.1209/0295-5075/85/30001>.
- [23] M. Abramowitz, I.A. Stegun, *Handbook of Mathematical Functions with Formulas, Graphs, and Mathematical Tables*, tenth printing, National Bureau of Standards Applied Mathematics Series, vol. 55, 1972.
- [24] F. Perey, B. Buck, A non-local potential model for the scattering of neutrons by nuclei, *Nucl. Phys.* 32 (1962) 353–380, [https://doi.org/10.1016/0029-5582\(62\)90345-0](https://doi.org/10.1016/0029-5582(62)90345-0), <https://www.sciencedirect.com/science/article/pii/0029558262903450>.
- [25] P. Descouvemont, D. Baye, The r-matrix theory, *Rep. Prog. Phys.* 73 (3) (2010) 036301, <https://doi.org/10.1088/0034-4885/73/3/036301>.
- [26] D. Baye, The Lagrange-mesh method, *Phys. Rep.* 565 (2015) 1–107, <https://doi.org/10.1016/j.physrep.2014.11.006>, <https://www.sciencedirect.com/science/article/pii/S0370157314004086>.
- [27] I.J. Thompson, Coupled reaction channels calculations in nuclear physics, *Comput. Phys. Rep.* 7 (4) (1988) 167–212.
- [28] I. Thompson, A. Barnett, Coulc: a continued-fraction algorithm for Coulomb functions of complex order with complex arguments, *Comput. Phys. Commun.* 36 (4) (1985) 363–372, [https://doi.org/10.1016/0010-4655\(85\)90025-6](https://doi.org/10.1016/0010-4655(85)90025-6), <https://www.sciencedirect.com/science/article/pii/0010465585900256>.
- [29] N. Michel, Precise Coulomb wave functions for a wide range of complex  $\ell$ ,  $\eta$  and  $z$ , *Comput. Phys. Commun.* 176 (3) (2007) 232–249, <https://doi.org/10.1016/j.cpc.2006.10.004>, <https://www.sciencedirect.com/science/article/pii/S0010465506003717>.
- [30] S. Elhay, J. Kautsky, Algorithm 655: Iqpack: Fortran subroutines for the weights of interpolatory quadratures, *ACM Trans. Math. Softw.* 13 (4) (1987) 399–415, <https://doi.org/10.1145/35078.214351>.
- [31] A. Koning, J. Delaroche, Local and global nucleon optical models from 1 keV to 200 MeV, *Nucl. Phys. A* 713 (3–4) (2003) 231–310.
- [32] Y. Han, Y. Shi, Q. Shen, Deuteron global optical model potential for energies up to 200 MeV, *Phys. Rev. C* 74 (2006) 044615, <https://doi.org/10.1103/PhysRevC.74.044615>, <https://link.aps.org/doi/10.1103/PhysRevC.74.044615>.
- [33] X.-W. Su, Y.-L. Han, Global optical model potential for alpha projectile, *Int. J. Mod. Phys. E* 24 (12) (2015) 1550092, <https://doi.org/10.1142/S0218301315500925>.
- [34] P. Descouvemont, An R-matrix package for coupled-channel problems in nuclear physics, *Comput. Phys. Commun.* 200 (2016) 199–219, <https://doi.org/10.1016/j.cpc.2015.10.015>, <https://www.sciencedirect.com/science/article/pii/S0010465515003951>.